

## Recent results in capillary discharge soft x-ray laser research

*J. J. Rocca, M.C. Marconi, Y. Wang, B.M. Luther, F. Pedacci, M. Grisham, G. Vaschenko, C.S. Menoni, J. Filevich, L. Juha<sup>(a)</sup>, Yu. P. Pershin<sup>(b)</sup>, E. N. Zubarev<sup>(b)</sup>, D. L. Voronov<sup>(b)</sup>, V. A. Sevryukova<sup>(b)</sup>, V. Kondratenko<sup>(b)</sup>, V. Shlyaptsev<sup>(c)</sup>, A. Vinogradov<sup>(d)</sup>, I. Artioukov<sup>(d)</sup>*

*NSF ERC for Extreme Ultraviolet Science and Technology and  
Department of Electrical & Computer Engineering, Colorado State University*

*<sup>(a)</sup>Institute of Physics (Czech Republic)*

*<sup>(b)</sup>Kharkov State Polytechnic University (Ukraine)*

*<sup>(c)</sup>University of California Davis at Livermore*

*<sup>(d)</sup>P.N. Lebedev Physical Institute (Russia)*

### Abstract

We report results of the development of capillary discharge driven metal-vapor plasma waveguides for the development of efficient laser-pumped soft x-ray lasers; and of the use of a previously developed capillary discharge Ne-like Ar 46.9 nm laser in study of the interaction of intense soft x-ray laser with materials. The guiding of a laser beam in a dense capillary discharge plasma channel containing a large density of Ag ions is reported. In term of applications we have conducted studies of materials modification and ablation with focalized 46.9 nm laser radiation at fluences between 0.1 and 100 J cm<sup>-2</sup>. The experiments demonstrated that the combined high repetition rate and high energy per pulse of the capillary discharge laser allows for the first time the processing of large surface areas with intense soft x-ray laser radiation. The damage threshold and damage mechanism of extreme ultraviolet Sc/Si multilayer mirror coatings was studied. Damage threshold fluences of ~ 0.08 J/cm<sup>2</sup> were determined for coatings deposited on both borosilicate glass and Si substrates. Scanning and transmission electron microscopy, and small-angle X-ray diffraction techniques revealed the thermal nature of the damage mechanism. These results provide a benchmark for the use of Sc/Si multilayer mirrors in high fluence applications, and for the development of higher damage threshold mirrors. Soft x-ray laser ablation studies were also conducted for silicon and several plastic materials, including PMMA, Polyamide and PTFE.

### I. Generation and characterization of a dense plasma waveguide with Ag ions.

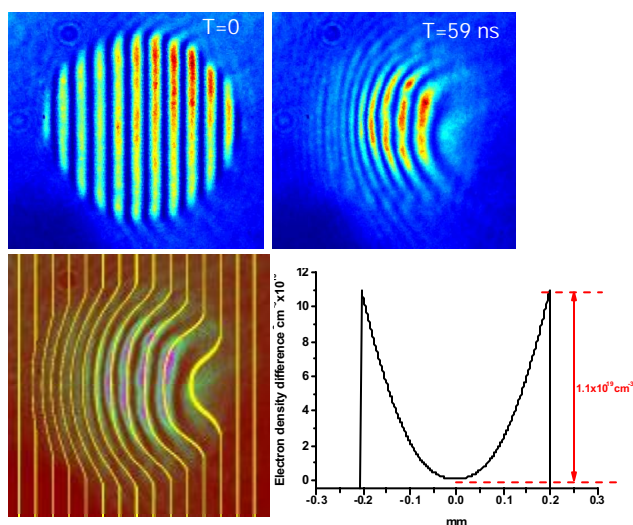
#### I.1 Introduction

The generation of dense plasma waveguides which can extend the interaction length between intense laser pulses and plasmas beyond the limits imposed by diffraction and ionization induced refraction is of significant interest for the development of efficient soft x-ray lasers. Several schemes for the generation of plasma waveguides based on either laser or discharge excitation have been studied [1-9]. Some of these plasma waveguides have been utilized in soft x-ray laser amplification experiments [10-12]. Picosecond laser excitation of sulfur plasma created by an ablative capillary discharge has been demonstrated to produce lasing at 60.8 nm in Ne-like S [10]. Laser amplification by electron ion recombination has been reported at 13.5 nm within plasma channels created by discharge or laser ablation of LiF micro-capillaries [11], and an optical-field ionization laser in Pd-like Xe at 41.8 nm is reported in these proceedings using a plasma channel created in a gas filled micro-capillary excited by a relatively slow discharge current pulse [12]. In another paper in these proceedings we report the generation and characterization of plasma waveguides in a highly ionized Ar plasma created by a fast capillary discharge of the type used to develop discharge-pumped collisional soft x-ray lasers [13]. All of the above soft x-ray laser amplification experiments have made use of plasmas generated from gases or from low Z materials. Herein we report the generation of dense plasma waveguides containing a large concentration of silver ions utilizing a fast (~ 55 ns first half-cycle) capillary discharge. The results are relevant to the development of a longitudinally excited Ag laser that takes advantage of transient collisional excitation [14,15]. The

longitudinal excitation of such lasers is of significant interest as it can potentially result in saturated amplifiers with reduced laser pump energy requirements and increased efficiency.

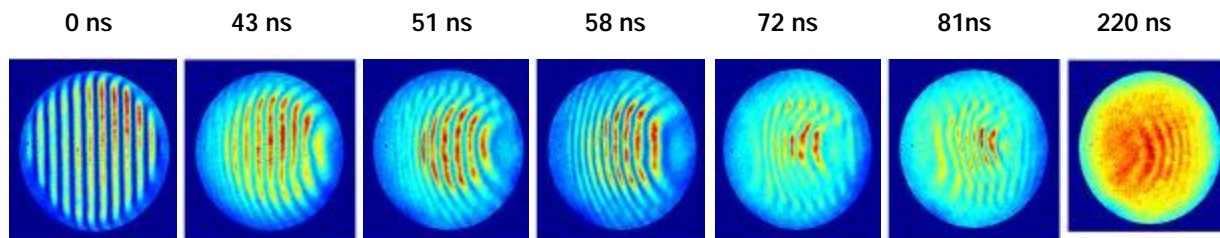
### I.1 Experimental Results

The plasmas were generated by discharge ablation of the walls of Ag<sub>2</sub>S capillaries 440 μm or 330 μm in diameter. The discharge current pulses had a peak amplitude of 3 to 5.5 kA and a half-period of ~ 55 ns. The plasma density distribution within the capillary was measured by sub-picosecond interferometry using the third harmonic (267 nm) of compressed ~ 1 mJ laser pulses from a Ti:Sapphire laser. Figure 1 (top right) shows an interferogram corresponding to a 440 μm diameter 2 mm long capillary excited by a 5.2 kA current pulse. It was obtained 59 ns after the initiation of the current pulse. A reference interferogram obtained prior to the initiation of the current pulse is shown in the top-left part of the figure. The lower-left part of the figure shows an overlay of the experimental data and a synthesized interferogram computed from an electron density profile that was adjusted to obtain a good fit of the experimental data. The electron density profile found by this procedure is shown in the bottom-right of the figure. The electron density difference is measured to be  $N_e \sim 1 \cdot 10^{19} \text{ cm}^{-3}$ .



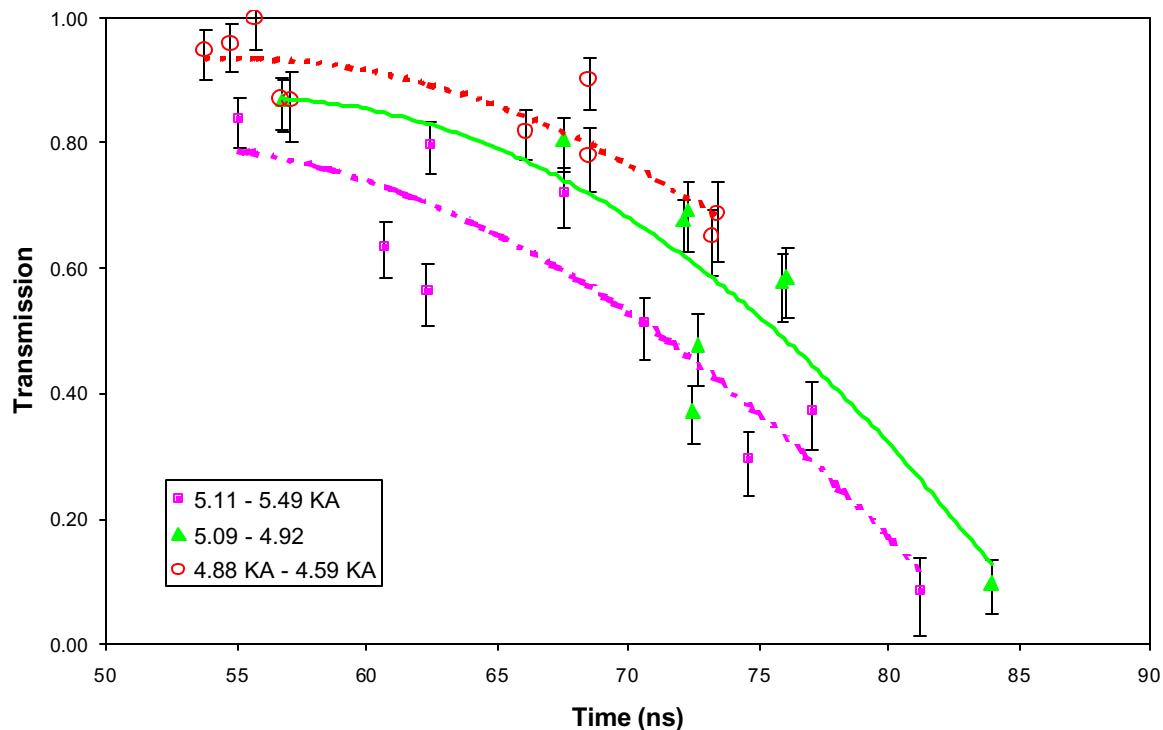
**Fig. 1.** Interferograms of 440 μm diameter, 2 mm long capillary discharge plasma excited by a 5.2 kA current pulse. The wavelength of the probe beam was 267 nm. a) Reference interferogram (no plasma present). b) Interferogram obtained 59 ns after the initiation of the current pulse. c) Overlay of measured and best-fit simulated interferogram. d) Corresponding radial variation of the electron density distribution. Notice that due to the absence of reliable reference fringes the interferograms yields the radial variation of the electron density, but not its absolute value. The on-axis electron density value was instead determined from absorption measurements.

Figure 2 shows a sequence of interferograms that map the temporal evolution of the electron density distribution within a 440 μm diameter Ag<sub>2</sub>S capillary. It was observed that at these discharge conditions the time span of interest for the generation of concave electron density profiles ranges from about 50 ns to 70 ns measured from the beginning of the current pulse. For times longer than ~ 70 ns, after the end of the first half-cycle of the current, the concave density profile starts to degrade rapidly. It is of interest to notice that late in time, after a few half-periods of the current ( e.g 220 ns frame in Fig. 2 ), the curvature of the fringes reverses direction.



**Fig. 2.** Sequence of interferograms corresponding to a 440 μm diameter capillary. The times are measured respect to the beginning of the current pulse.

It should be noticed that the absolute value of the electron density on axis can not be determined from these data due to the difficulty of reliably determining the position of the “zero density” fringes. This is due to the fact that nowhere within the capillary channel the electron density is zero, added to the additional complication that the position of the fringe in the reference interferograms obtained in the absence of a plasma (first frame in fig.2) changes from shot to shot. The electron density on axis was instead determined measuring the absorption of a 267 nm probe beam of ~ 100 um diameter propagated along the capillary axis. The probe beam was focused into a spot at the entrance of the capillary and was made collinear with the capillary axis. The measured beam transmissivity as a function of time respect to the origin of the current pulse is shown in Fig. 3 for three different ranges of current pulse amplitudes. Assuming from hydrodynamic model computations an electron temperature of 20 eV and mean ionization of  $Z=8.6$ , and neglecting fringe effects, the measured absorptions for the majority of the shots within the time interval corresponding to the formations of strongly guiding density profiles ~ (50-70 ns) amount to axial electron densities of  $\sim 2\text{-}3 \times 10^{19} \text{ cm}^{-3}$ .



**Fig. 3.** Transmissivity of 267 nm beam through the axis of a 2.2 mm long 440 um diameter  $\text{Ag}_2\text{S}$  capillary plasma excited by a 55 ns half-period current pulse. Data for three different ranges of peak currents is shown. The error bars represent the uncertainty in determining the transmissivity of each individual shot. The scatter in the data illustrates the shot to shot variations. Variations in absorption were also observed from one capillary to another.

Smaller diameter capillaries were measured to generate plasmas with steeper density walls and with higher density on axis. Fig. 4 shows an interferogram and corresponding electron density profile for a 330  $\mu\text{m}$  diameter capillary excited by a 3.3 kA current pulse. The interferogram was obtained 57 ns after the initiation of the current pulse. The electron density gradient and the “walls” of the waveguide are larger than those measured for the 440  $\mu\text{m}$  diameter capillary.

Modeling of the guiding characteristics of these plasmas was accomplished by first determining a radially dependent phase delay based on the interferometrically measured electron density profiles, and subsequently propagating the beam using a fast-Fourier transform method. The measured electron density profile for a 440  $\mu\text{m}$  diameter capillary shown in Fig. 1 is computed to guide a beam with a matched mode size of  $\omega_0 = 25 \mu\text{m}$ . Beam propagation experiments were conducted focusing 180 ps duration, 100 mJ pulses from the second stage of the Ti:Sapphire laser at the entrance of the

capillary channel into a  $2\omega_0$  - 60  $\mu\text{m}$  spot, and imaging the output onto a CCD camera. The laser pulses were generated with a Kerr lens mode-locking Ti:Sapphire oscillator, stretched to  $\sim 180$  ps and subsequently amplified in a two stage Ti:Sapphire amplifier system. Fig. 4 shows exit mode patterns corresponding to a 440  $\mu\text{m}$  diameter, 4 mm long capillary, acquired 55 ns after the initiation of the current pulse. Fig. 4a shows an output mode pattern with a well defined peak of  $\sim 54$   $\mu\text{m}$  FWHM and a relatively low pedestal. However, we also observed shot-to-shot variations in the exit beam intensity distribution, with some shots showing a significantly more spread exit beam distribution such as that in Fig. 4b.

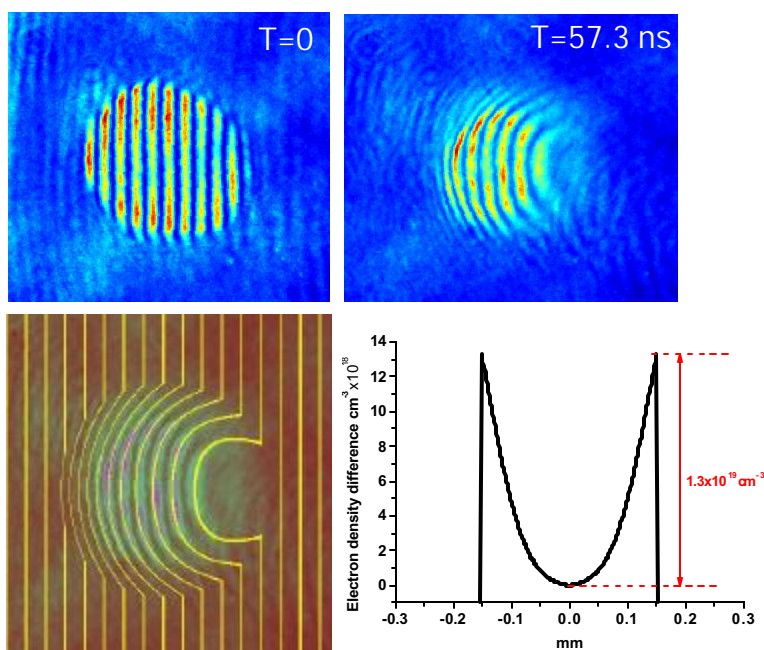


**Fig. 4.** Interferograms of 330  $\mu\text{m}$  diameter, 2 mm long capillary discharge plasma excited by a 3.1 kA current pulse. The wavelength of the probe beam was 267 nm. a) Reference interferogram (no plasma present). b) Interferogram obtained 57.3 ns after the initiation of the current pulse. c) Overlay of measured and best-fit simulated interferogram. d) Corresponding radial profile of the electron density distribution. Notice that due to the absence of reliable reference fringes the measurements yield the radial variation of the electron density, but not its absolute value. The on-axis electron density was separately determined from absorption measurements.

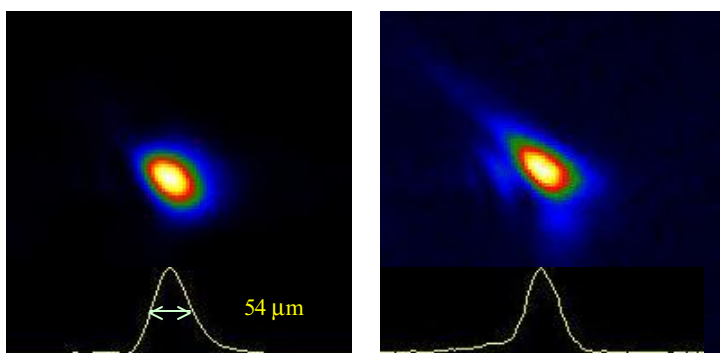


**Fig. 5.** Exit beam intensity distribution patterns corresponding to a Ti:Sapphire laser beam propagated through a 440  $\mu\text{m}$  diameter, 4 mm long capillary. The laser pulse had an energy of 100 mJ and a pulse duration of 180 ps.

The evolution of these capillary discharge plasmas was simulated using the code RADEX, as discussed in the paper by V.N. Shlyaptsev et al in these proceedings. The computed electron density profile are in good agreement with those measured by interferometry and clearly corroborate the guiding characteristics of these discharges. In summary the results presented above demonstrate the generation of dense plasma waveguides in a relatively high Z metal vapor plasmas of interest for collisional soft x-ray lasers.

## II. MATERIALS MODIFICATION STUDIES WITH A HIGH REPETITION RATE SOFT X-RAY LASER

Materials processing with optical lasers is an active and well established field. In contrast, materials modification with soft x-ray light is a new area only now made possible by the recent development of intense high repetition rate soft x-ray sources. In these proceedings we report results of materials modifications studies conducted utilizing a 46.9 nm Ne-like Ar capillary discharge laser emitting pulses of  $\sim 1.2$  ns duration. The large energy per pulse and large repetition rate of this source allows for the first time the processing of relatively large areas of material. As an example Fig. 6a shows an area of several millimeter square of a Sc/Si multilayer film that has been processed with 46.9nm nanosecond laser pulses with a fluence of  $\sim 0.2$  J cm<sup>-2</sup>. This type of large area processing has allowed for X-ray diffraction studies of the modified materials. Experiments were conducted to study the interaction of intense 46.9 nm nanosecond laser pulses with several plastic materials, silicon, and the Sc/Sc multilayer films used for the fabrication of mirrors at operating at wavelengths between 30 nm and 50 nm.. The determination of the damage threshold and damage mechanism of these multilayer is of significant interest for their use with soft x ray-ray lasers, as they provide the highest reflectivity available at this wavelength range [16,17].

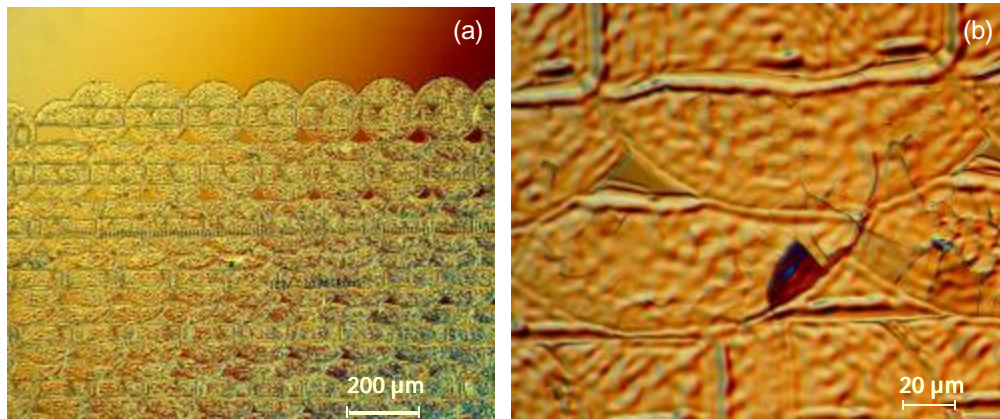


**Fig.6.** Sc/Si multilayer film irradiated with 46.9 nm laser pulses of  $\sim 1.2$  ns duration from a Ne-like Ar capillary discharge laser at a fluence of  $0.5$  J cm<sup>-2</sup>. a) Large area processed scanning the sample in front of the focused soft x-ray laser beam. b) Image showing a magnified fraction of the processed film shown in(a).

The experimental setup used to irradiate the samples is schematically shown in Fig.7, and resembles that previously used with the laser to study the ablation of several metals with focused soft x-ray laser radiation [18]. The laser emission was focused onto the target surface with a spherical  $R = 10$  cm Sc/Si multilayer-coated mirror 2.5 cm in diameter positioned at normal incidence. The reflectivity of the particular mirror used in this experiment was measured to be  $\sim 30\%$  at 46.9 nm. The capillary-discharge Ne-like Ar laser used as a source of soft x-ray radiation was configured to produce pulses with an energy of  $\sim 0.13$  mJ and  $\sim 1.2$  ns FWHM duration [19]. The far-field laser beam profile has an annular shape with a peak-to-peak divergence of about 4.6 mrad. The Sc/Si multilayer samples were cut to a  $3 \times 5$  mm size and mounted on a 1.6 mm thick brass strip holder located at 1.45 m from the exit of the laser. As illustrated in Fig. 7 the sample and the holder block a fraction of the laser beam, which in that plane has a diameter of  $\sim 13$  mm. Motorized translation stages were used to allow for the translation of the sample along an axis that forms an angle of  $\sim 50^\circ$  with respect to the laser beam, and for its accurate positioning in the horizontal and vertical directions. The displacement of the samples along this angle allowed us to vary the distance between the sample and the focal spot to select EUV radiation fluences between  $\sim 0.01$  and  $150$  J/cm<sup>2</sup>, while simultaneously changing the target area intersected by the beam after each shot. In some samples individual spots were irradiated by single laser shots, whereas in others a large number of shots were used to irradiate  $2 \times 2$  mm<sup>2</sup> areas with a fixed fluence to allow for X-ray diffraction studies of thin damaged films. These large area exposures (Fig.6b) were accomplished by scanning the sample in the horizontal and the

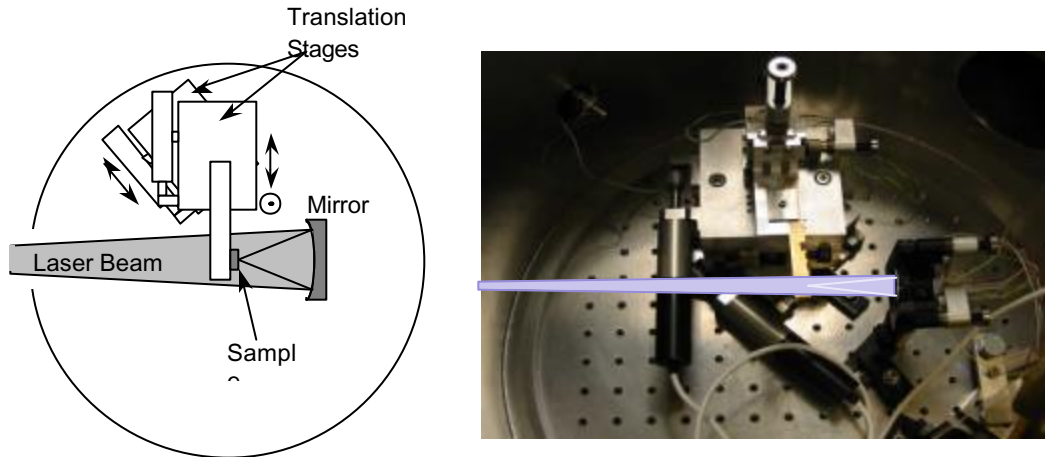


Fig.7. Schematic of the ablation set up used to investigate the damage threshold of Si/Sc multilayers

vertical directions in front of the laser beam to overlap each individual irradiated zone, while firing the laser at a repetition rate of 1 Hz.

## II. 1 Ablation of plastic materials

Ablation studies were conducted for several plastic materials including PMMA, Polyamide, and PTFE. Samples were processed varying the irradiation fluence and the number of shots. The results were compared with similar studies conducted by L. Juha et al. on the same type of samples using 86 nm, 50 fs duration pulses of  $\sim 5 \mu\text{J}$  energy produced by the Tesla free-electron laser (FEL) facility [20]. As an example Fig. 8 shows ablation results obtained with the 46.9 nm capillary discharge laser for PMMA. The ablation efficiency of PMMA as a function of the number of laser shots is shown in Fig. 3. Comparison with results obtained with the FEL show that the ablation efficiency of ns 46.9 nm pulses is similar to 86 nm pulses of 50-100 fs duration at the same irradiation fluence. A more detail discussion of the ablation results for different plastics will be published elsewhere.

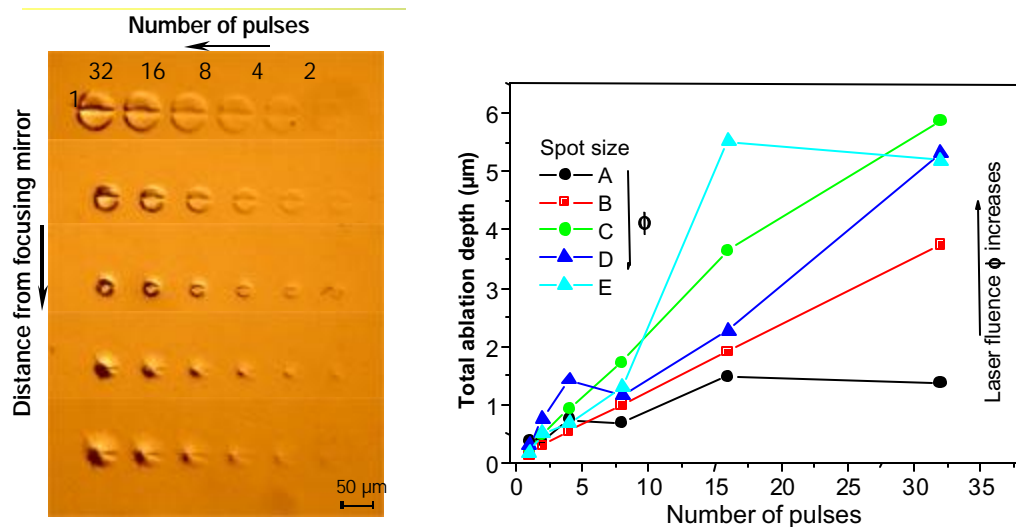
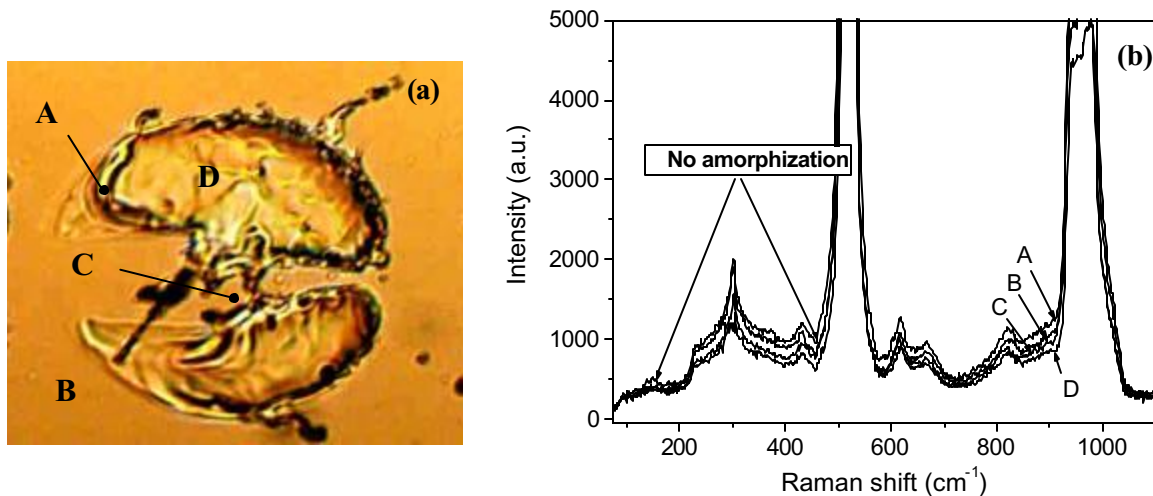


Fig. 8. (a) Results of ablation of PMMA with  $\sim 1.2$  ns pulses of 46.9 nm radiation at different fluences as a function of the number of laser shots. (b) Efficiency of PMMA ablation versus the number of shots for fluences  $\phi = 1.4, 4.1, 12.4, 50$  and  $140 \text{ J cm}^{-2}$

## II.2 Irradiation of Silicon

Fig. 9 shows the ablation crater (a) and corresponding micro-Raman spectra (b) resulting from irradiation of silicon with 46.9 nm laser pulses at a fluence of  $\sim 5.5 \text{ J/cm}^2$ . The ablation depth at this fluence is found to be approximately 1  $\mu\text{m}$  per pulse. The smallest laser emission fluence required to produce any detectable damage on the silicon surface was found to be  $\sim 0.7 \text{ J/cm}^2$ , which is significantly higher than the damage threshold of the ScSi multilayer mirror coatings investigated in this work. Unlike the ablation of PMMA, the 46.9 nm irradiation of silicon causes material expansion. However, as follows from the micro-Raman investigation (Fig. 9(b)), only small amounts of silicon in the ablated area are amorphized. This is in contrast to the recently reported heavy amorphization in ablation experiments with femtosecond pulses at 86 nm produced by the free-electron laser at the Tesla test facility.



**Fig.9.** Micrograph (a) and micro-Raman spectra (b) of an ablation spot on surface of Si wafer obtained by irradiation with  $5.5 \text{ J/cm}^2$  pulsed laser emission at 46.9 nm. Different spectra shown in (b) were obtained in different areas of the ablation spot as labeled by the capital letters.

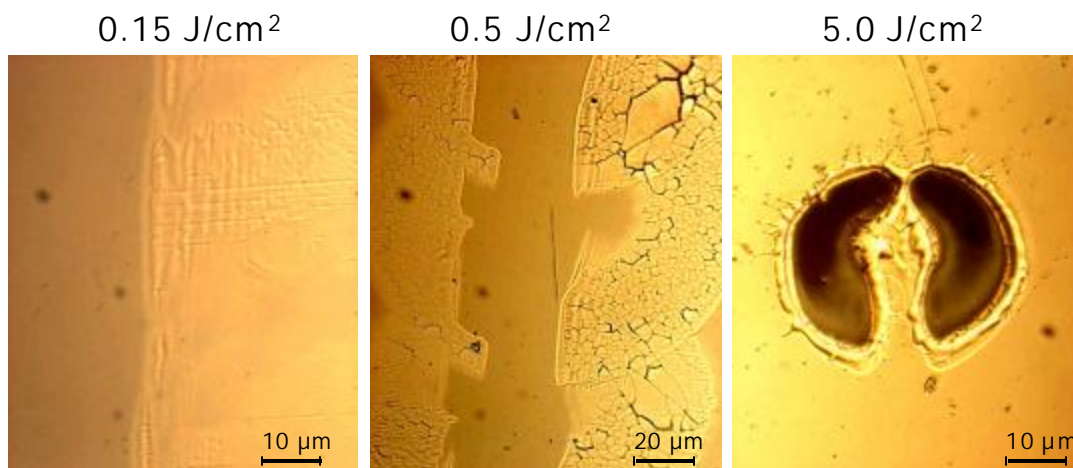
## II. 3 Study of the damage threshold and damage mechanism of soft x-ray multilayer mirrors exposed to intense 46.9 nm laser pulses

High reflectivity mirrors with high damage threshold are key elements for enabling applications of soft x-ray laser sources and other newly developed high fluence sources such as free-electron lasers. Significant progress has been made in the developing of high reflectivity Sc/Si mirrors for the 35-50 nm range [16] with reflectance values as high as 43 percent in the vicinity of 47 nm [17]. However, the damage threshold of these mirrors when exposed to high peak powers of EUV light has not been studied. This is now particularly important as the peak power and fluence of soft x-ray sources have reached unprecedented values. For example the radiation fluence at the exit of the plasma column in capillary discharge Ne-like Ar lasers operating at 46.9 nm can exceed  $1 \text{ J/cm}^2$  [21].

We have studied the optical damage mechanisms and damage threshold of Sc/Si EUV (35-50 nm range) mirrors exposed to high power soft x-ray laser radiation. The study was conducted by focusing the output of a tabletop capillary-discharge Ne-like Ar laser emitting nanosecond duration pulses at a wavelength of 46.9 nm. The resulting damage of the coatings exposed to fluences ranging from 0.01 to  $10 \text{ J/cm}^2$  was analyzed with optical microscopy, scanning electron microscopy (SEM), transmission electron microscopy (TEM), and with small-angle X-ray diffraction ( $\lambda=0.154 \text{ nm}$ ) techniques. Our results show similar values of damage threshold of  $\sim 0.08 \text{ J/cm}^2$  for Sc/Si multilayer coatings on Si and

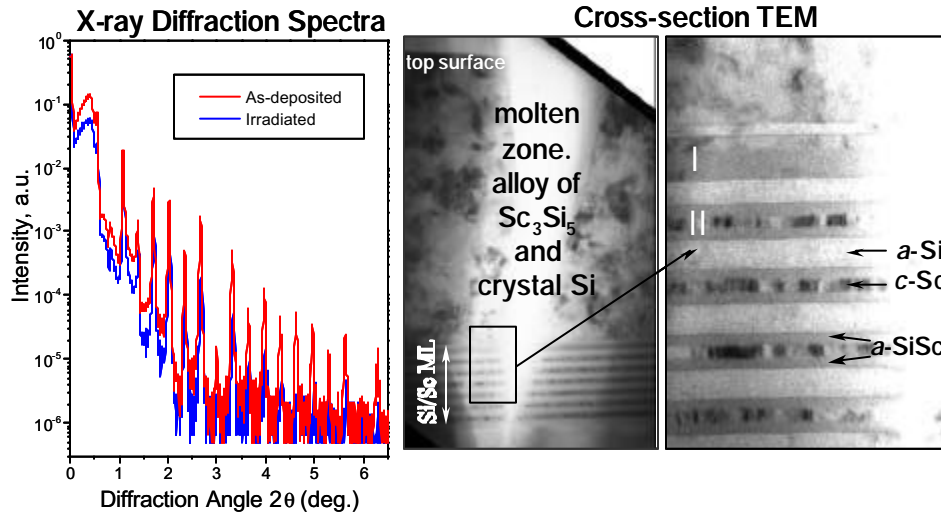
SiO<sub>2</sub> substrates, compared to 0.7 J/cm<sup>2</sup> found necessary to damage a bare Si substrate. The Sc/Si multilayers were deposited by dc-magnetron sputtering at 3 mTorr of Argon pressure on superpolished borosilicate glass (surface roughness  $\sigma \sim 0.4$  nm) and on silicon wafers ( $\sigma \sim 0.6$  nm). The multilayers on borosilicate glass consisted of 10 periods of Sc/Si layers, each with a thickness of  $\sim 26.7$  nm, and a ratio of layer thickness H(Sc)/H(Si)  $\sim 0.7$ . A top protection layer of Si of thickness  $\sim 5$  nm capped the multilayers. The multilayer coatings deposited on Si consisted of 33 periods of Sc/Si pairs with the same parameters as the borosilicate glass ones. In these structures the crystalline Sc layers are always separated from the amorphous Si layers by  $\sim 3$  nm of amorphous ScSi interface layers formed by interdiffusion [22].

Fig. 10 shows typical SEM images of damaged areas of coatings deposited on a Si wafer resulting from average EUV fluences of 0.15 J/cm<sup>2</sup> (a), 0.5 J/cm<sup>2</sup> (b) and 5 J/cm<sup>2</sup> (c). At 0.15 J/cm<sup>2</sup> (Fig. 10 (a)) and lower fluences we observe large areas with discoloration and undulations of the coating. These areas are most likely produced by heat-triggered interdiffusion in the upper layers of the coatings. This surface modification, which already appears at fluences of  $\sim 0.08$  J/cm<sup>2</sup>, establishes the damage threshold for the Sc/Si multilayers defined in this work. In comparison, the onset of damage in bare Si substrates measured in this work appears at significantly larger irradiation fluence of 0.7 J/cm<sup>2</sup>. The areas with larger local fluences (Fig. 10(b)) are covered with cracks resulting from significant mechanical tensile stress generated by thermal expansion and the following cooling down process [8]. At even larger fluences of  $\sim 5$  J/cm<sup>2</sup> the coating is fully evaporated from the center of the irradiated spot and the Si substrate is also damaged (Fig. 10 (c)). Electron microanalysis data reveals that Sc is absent in the center part of the dark region shown in Fig. 10 (c).



**Fig.10.** SEM micrographs of the damaged areas of the Sc/Si coatings exposed to EUV laser beam fluences of 0.15 J/cm<sup>2</sup> (a), 0.5 J/cm<sup>2</sup> (b), and 5 J/cm<sup>2</sup> (c).

Small-angle X-ray diffraction analysis of the samples with  $2 \times 2$  mm<sup>2</sup> area irradiated with  $\geq 0.1$  J/cm<sup>2</sup> emission fluence shows a noticeable drop in the intensity of the diffraction peaks with respect to the unexposed areas. Thus a sample irradiated with a fluence of  $\sim 0.13$  J/cm<sup>2</sup> loses 20-30% and a sample processed with a fluence of  $\sim 0.21$  J/cm<sup>2</sup> (Fig. 11(a)) loses 75-85% in the diffracted intensity. However, the peak's position remains approximately the same, indicating that the coating is only partially destroyed. This evidence suggests that while at these fluences the top layers of the coating are melted, the layers adjacent to the substrate remained unchanged. This interpretation of the X-ray diffraction data was confirmed by cross-section TEM imaging of the sample exposed at 0.21 J/cm<sup>2</sup>. The TEM image of Fig. 4b shows that the top 700 nm of the coating are molten, while  $\sim 180$  nm (7 periods) adjacent to the substrate are not destroyed. The molten layer constitutes an alloy of Sc<sub>3</sub>Si<sub>5</sub> and crystal Si as determined from electron diffraction data. Analysis of the surviving multilayer coating beneath the molten layer indicates that changes in layer thickness have occurred within a distance of less than 2 periods from the molten region (Fig. 11(b)), thus the heat affected zone (HAZ) did not exceed  $\sim 50$  nm.



**Fig. 11.** (a) Cross-sectional TEM image of the molten zone and (b) survived layers (magnified) of a Sc/Si multilayer sample irradiated with 0.21 J/cm<sup>2</sup> pulses of 46.9 nm laser radiation.

Comparison of the layer structure in the HAZ with that of isothermally annealed samples indicates that the various stages of structural and phase transformations observed within a few periods of the coating under laser irradiation are the same as in samples annealed at different temperatures. Both structural and phase transformations in Si/Sc multilayers at temperatures up to 970 °C have been previously studied in detail [23, 24]. The changes taking place in the Sc-containing layer nearest to the molten region (indicated by I in Fig. 8b) correspond to a stage of formation and crystallization of Sc<sub>3</sub>Si<sub>5</sub> silicide that have been observed in isothermally annealed coatings at 430 °C after 1 hour. In the next Sc-containing layer (indicated by II in Fig. 8b) only minor expansion of the ScSi silicide interface layers is observed, which is a result of solid state amorphization. Similar effects have been observed at annealing temperatures of less than 200 °C [23,24]. These results provide a benchmark for the use of Sc/Si multilayer mirrors in high fluence applications, and for the improvement of high damage threshold soft x-ray mirrors.

### III.4 Laser-induced periodic surface nano-structures generated by a 46.9 nm laser

The formation of periodic surface structures on surfaces by laser light with wavelengths ranging from the visible to the mid-infrared has been extensively studied [25]. In those cases the scale length of the patterns, which is proportional to the wavelength of the light, is typically in the micrometer scale. We have used a 46.9 nm tabletop capillary discharge laser to generate laser-induced periodic surface structures with nanoscale dimensions. Figure 12 shows linear structures broken into a pearl chain obtained in PMMA. The distance between the neighboring lines is 60 nm. A more detail discussion of these results will be published separately.

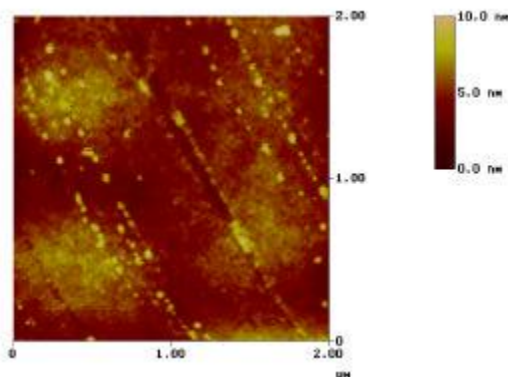


**Fig. 12.** AFM topographic image of PMMA surface irradiated with a 46.9 nm capillary discharge laser. Linear structures broken into a pearl chain can be seen on the surface. The distance between the neighboring lines is ~ 60 nm.

**Acknowledgments.** This work was supported in part by the Engineering Research Centers Program of the National Science Foundation under NSF Award Number EEC-0310717 and by the U.S Department of Energy, Chemical Sciences, Geosciences, and Biosciences Division of the Office of Basic Energy Sciences. We also gratefully acknowledge the support of the W.M. Keck Foundation.

## References

1. C.G. Durfee III and H.M. Milchberg, Phys. Rev. Lett. **71**, 2409, (1993); C.G. Durfee III, J. Lynch and H.M. Milchberg, Phys. Rev. E, **51**, 2368, (1995)
2. Y. Ehrlich, C. Cohen, A. Zigler, J. Krall, P. Sprangle and E. Esarey, Phys. Rev. Lett, **77**, 4186, (1996)
3. J.J. Rocca, F.G. Tomasel, J.L.A. Chilla, C.H. Moreno, B.R. Benware, V.N. Shlyaptsev, J.J. Gonzalez and C.D. Macchietto. SPIE vol **3156**, 164, (1997).
4. M.C. Marconi, C.H. Moreno, J.J. Rocca, V.N. Shlyaptsev and A.L. Osterheld, Physical Review E **62**, 7209, (2000).
5. S.M. Hooker, D.J. Spence and R.A. Smith; J. Opt. Soc. Am B, **17**, 90 (2000)
6. Butler, D.J. Spence and S.M. Hooker, Phys. Rev. Lett, **89**, 185003, (2002)
7. T. Hosakai, M. Kando, H. Dewa, H. Kotaki, S. Kondo, N. Hasagawa, K. Nakajima, K. Horioka, Opt. Lett, **25**, (2000)
8. C. Fauser and H. Langhoff. Appl. Phys. **B 71**, 607, (2000)
9. B. Luther, Y. Wang, M.C. Marconi and J.J. Rocca, p 332 "X-Ray Lasers 2002". AIP Conf. Proc. 641. Eds. J.J. Rocca, J. Dunn and S. Suckewer (2002).
10. K. A. Janulewicz, J. J. Rocca, F. Bortolotto, M. P. Kalachnikov, V. N. Shlyaptsev, W. Sandner, and P. V. Nickles, Phys Rev. A **63**, 033803 (2001).
11. D. Korobkin, C.H. Nam, S. Suckewer, and A. Goltsov. Phys. Rev. Lett. **77**, 5206, (1996)
12. A. Butler, A.J. Gonsalves, C.M.M. Kenna, D.J. Spence, S.K.M. Hooker, S. Sebban, T. Mocek, I. Bettaivi and B. Cross, in these proceedings.
13. B. Luther, Y. Wang, M.C. Marconi, M. Berrill, D. Alessi, J.L.A. Chilla and J.J. Rocca, in these proceedings.
14. P.V. Nickles, M. Schnuerer, M.P. Kalashnikov, I. Will, W. Sandner, and V.N. Shlyaptsev. Phys. Rev. Lett. **78**, 2748, (1997).
15. J. Dunn, Y. Li, A. L. Osterheld, J. Nilsen, J. R. Hunter, and V. N. Shlyaptsev, Phys.Rev.Lett. **84**, 4834-4837 (2000).
16. Yu. A. Uspenskii, V. E. Levashov, A. V. Vinogradov, A. I. Fedorenko, V. V. Kondratenko, Yu. P. Pershin, E. N. Zubarev, and V. Yu. Fedotov, Opt. Lett. **23**, 771 (1998).
17. J. J. Rocca, M. Frati, B. Benware, M. Seminario, J. Filevich, M. Marconi, K. Kanizay, A. Ozols, I. A. Artiukov, A. Vinogradov, and Y. A. Uspenskii, C. R. Acad. Sci. IV-Phys. **1**, 1065 (2000).
18. B. Benware, A. Ozols, J.J. Rocca, I.A. Artiukov, V.V. Kondratenko and A.V. Vinogradov Optics Lett. **24**, 1714, (1999).
19. B. R. Benware, C. D. Macchietto, C. H. Moreno, and J. J. Rocca, Phys. Rev. Lett. **81**, 5804, (1998).
20. Ayvazyan *et al.*, Phys. Rev. Lett. **88**, 104802 (2002).
21. C.D. Macchietto, B.R. Benware and J.J. Rocca, Optics Lett. **24**, 1115, (1999).
22. Fedorenko, Yu. P. Pershin, O. V. Poltseva, A. G. Ponomarenko, V. S. Sevryukova, D. L. Voronov and E. N. Zubarev, J. X-ray Sci. Technol. **9**, 35 (2001).
23. D. L. Voronov, V. V. Kondratenko, E. N. Zubarev, A. V. Pen'kov and Yu. P. Pershin, Functional Materials **9**, 534 (2002).
24. D. L. Voronov, E. N. Zubarev, V. V. Kondratenko, A. V. Penkov, Y. P. Pershin, A. G. Ponomarenko, I. A. Artiukov, A. V. Vinogradov, Y. A. Uspenskii, and J. F. Seely, AIP Conf. Proc. **641**, 575 (2002).
25. D.B. Chrisey and G.K. Hubler , Eds. , "Pulsed Laser Deposition of Thin Films", Eds., John Wiley & Sons, pp. 90 (1994).